CHIRON CCD detector: tests in March 2011

A. Tokovinin

Version 3. March 28, 2011
file: prj/bme/chiron/dewar/reports/report-Mar6.tex

1 Summary of recent work

The CHIRON CCD detector system has been delivered to the telescope in January 2011 with numerous shortcomings which have not allowed its science use. Starting mid-February, P. Moore and M. Bonati worked on the controller. The clocking sequence has been changed, the hardware problem in the lower-right readout channel was diagnosed. The system was configured to read through two amplifiers, upper-left and upper-right.

After the discovery of strong non-linearity on February 19 and its subsequent confirmation, the system was moved to La Serena on February 23. It turned out that the source of the non-linearity was the Monsoon Orange acquisition board.[1] After installing the boards from the previous Monsoon controller (the one used with echelle throughout 2010), the linearity and noise performance have improved. Uncontrolled horizontal shifts of the image were encountered and corrected in the first week of March.

During these tests, the acquisition program was writing 32-bit images, making use of the full 18-bit dynamic range of Monsoon. In the final configuration tested here, only the 16 least significant bits are written. The numerical saturation at 2^{16} occurs already on the highly non-linear part of the response.

P. Moore has increased the dwell time to 1 μs and reached low noise in this *normal* readout mode. Then he implemented the *fast* mode with pixel frequency of 440 kHz, almost as fast as the originally delivered 500-kHz readout. The binning and ROI were also programmed and tested by P. Moore and M. Bonati. The last change to the system was made on March 4 in the afternoon, when Peter has modified the Monsoon to increase the drain and gate voltages on the CCD, in hope of improving the linearity.

2 Test setup

The system was tested during various stages of this work. This document presents the results of tests conducted on March 5, 2011 (with addition of further tests where necessary). The detector was located in the La Serena detector room, where a test image could be projected on it. The light source was a current-stabilized LED. The system was connected to the `ctiola` computer and controlled by the

[1] P. Moore wrote on February 24: "I therefore surmise that the video processor chain modifications that were made in Tucson to make this particular board optimal for Chiron were in fact incorrect."

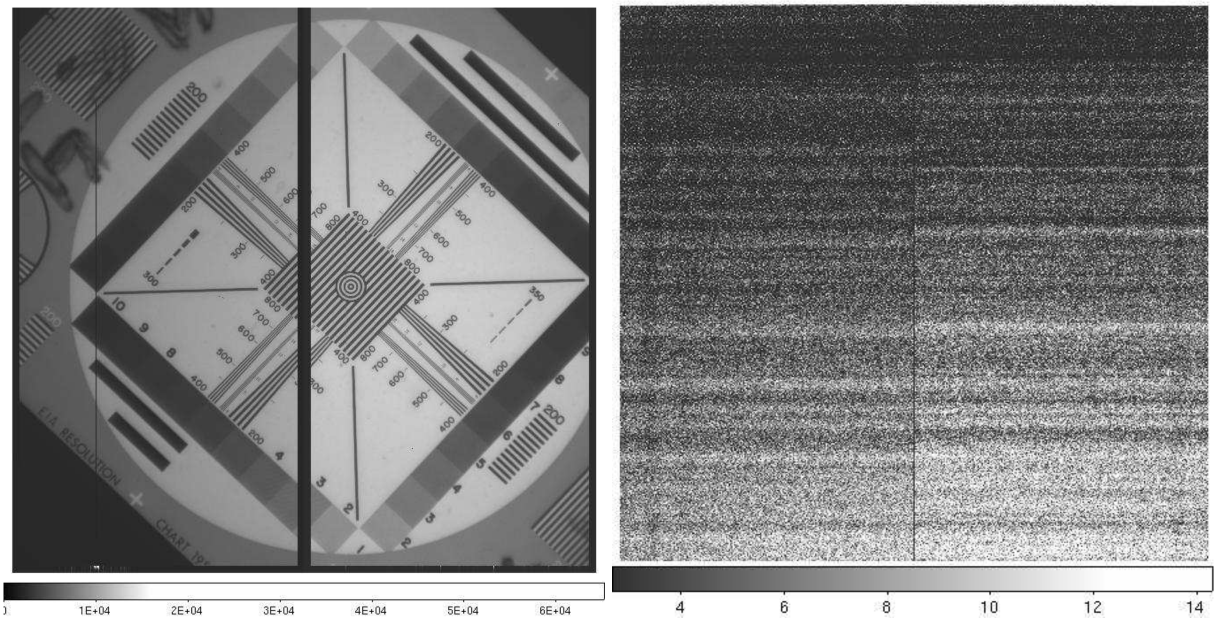

Figure 1: Left: raw image ft0037 (1x1 binning, full frame, fast mode). Right: bias image ft0033, overscan-subtracted and trimmed (2x2 binning, normal mode).

same software as used in CHIRON. The user interface, however, was different (an engineering GUI). Changing readout speed, binning and ROI was done by commands listed below.

```
pan appmacro speed_normal [speed_fast]
pan set modifier yoverscan <value>
set_binning Nx Ny
set_roi xstart ystart xsize ysize
set_roi full
```

The test data are located in `/data/20110305/` directory on `ctiola`. Figure 1 (left) illustrates the raw test image, with black vertical stripes corresponding to the pre-scan and overscan areas. The 50-pixel vertical overscan was used in these tests, creating a dark horizontal band below the image, filled with vertical “streaks”.

The trimmed bias image is shown in Figure 1 (right). It was taken with 2x2 binning in the normal mode. There was some weak residual detector illumination. During 14-s readout time the parasite light accumulates, causing the intensity increase by $\sim$ 10 ADU in the lower part of the image. In the upper 500 lines used for the linearity test, this extra signal does not exceed 3 ADU. When we cover the detector with a black cloth, the bias frames do not have this vertical gradient (see /data/20110304/tst0126.fits). The horizontal “bands” in the bias image are caused by the low-frequency component of the readout noise (see below).

3 Linearity

The projected image was covered by 3 layers of white paper to get a smooth and faint illumination of the detector. Series of images with exposure time from 0.5s to 30s were taken with 2x2 binning (to speed up the readout).

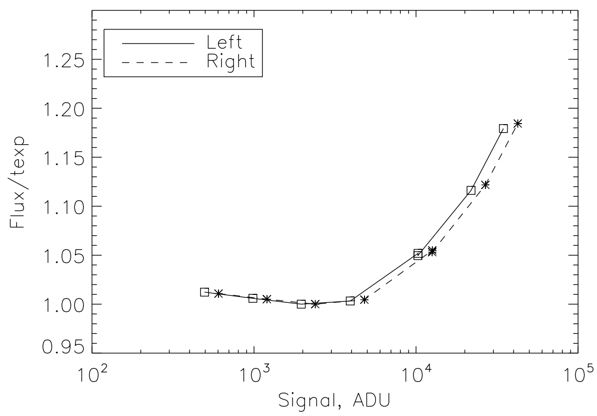

Figure 2: Linearity in the normal readout mode. Left: measurements, right: after correction.

The data were processed by the IDL program `lin1.pro`. On a well-exposed image, all pixels illuminated at a level from 0.8 to 0.97 of maximum in the upper 500 lines are selected for flux measurement. This mask is constructed separately for each of the two CCD halves (left, right) and applied to all exposures to calculate the flux. The median overscan value is subtracted in flux calculation. The ratio of flux to exposure time is plotted vs. average signal level. This ratio is normalized by its minimum value (Figs. 2 and 3).

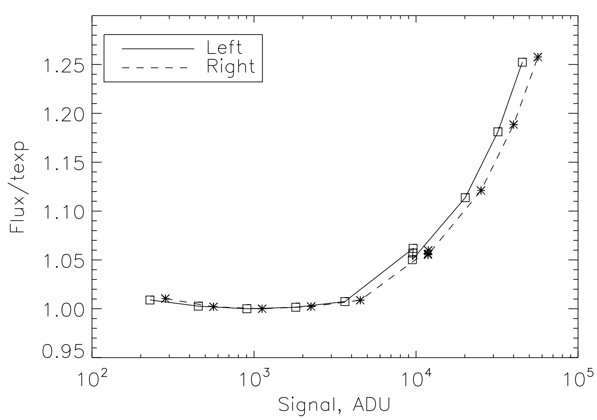

Figure 3: Linearity in the fast readout mode. Left: measurements, right: after correction.

Measurements in the fast and normal modes show similar trends and are discussed jointly. At strong signal, the "positive" non-linearity is seen. This is similar to the non-linearity of the original acquisition boards[2], but amounts only to 20%, instead of a factor of two.

The increase at low light levels appears to be an artifact of the test setup. LEDs have negative temperature coefficient and tend to give more light immediately after switching on, until they worm up. Sub-percent changes in flux between two 10-s exposures can be also caused by the LED heating. Parasite light could also cause an upturn at low levels, but it was too weak (<3 ADU) to explain the observed upturn.

A simple quadratic correction

$$S_{corr} = S\,(1 - kS) \tag{1}$$

can remove most of the observed non-linearity, as can be seen in Figs. 2, 3. We use the *non-linearity coefficients* k of $[4.5, 4.0] \times 10^{-6}$ in the normal mode and $[5.0, 4.3] \times 10^{-6}$ in the fast mode. The relative deviation from linearity is about Sk, reaching 10% at $S \sim 25$ kADU. Tests on March 2, 2011 (before increasing the voltages) have resulted in $k = [3.9, 2.9] \times 10^{-6}$. Therefore, after increasing the drain voltages the non-linearity has not improved.

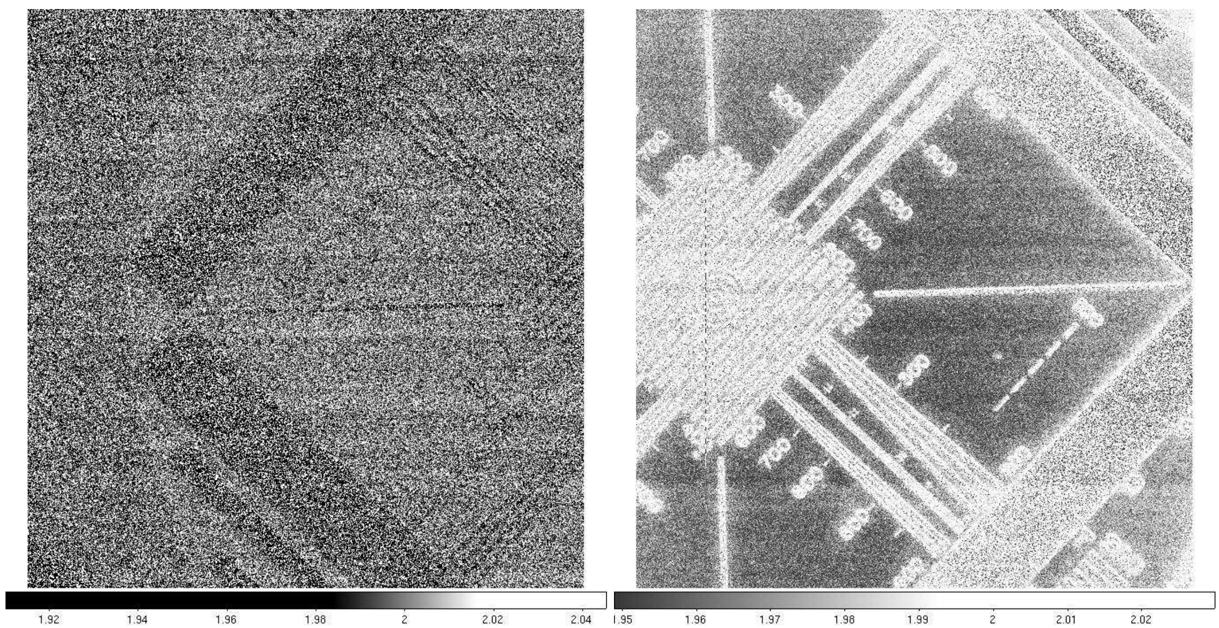

Figure 4: Ratios of images with double exposure time, after non-linearity correction. Fragments of right-quadrant images near the center. Left: ft0036/ft0037, 2s/1s, max. signal 24kADU. Right: ft0035/ft0036, 4s/2s, max. signal 50kADU. Fast mode, no binning.

A stringent test of the linearity is a constant ratio of two images taken with different exposures. The program `ratio3.pro` calculates this ratio (separately for each amplifier) and saves the resulting ratio image in a FITS file. The signals are corrected for the non-linearity by (1). For signal levels up to 20 kADU the ratio is indeed "flat", at higher signal levels the ratio shows a negative trace of the image because the corrected response turns down (see Fig. 3, right).

[2]See "Linearity and gain of the CHIRON CCD detector", February 19, 2011

4 Gain and noise

Fluctuations of the ratio r of two images allow us to measure the gain g [electrons per ADU]. First, we subtract from the measured variance of the ratio σ_r^2 the RON contribution

$$\sigma_0^2 = \sigma_r^2 - (R_{ADU}/S)^2(1 + r^2) \tag{2}$$

using R_{ADU} calculated from the over-scan region. Then the gain is estimated as

$$g = r(1 + r)/(\sigma_0^2 S). \tag{3}$$

This translates to a trivial result $g = 2/(\sigma_0^2 S)$ for the ratio of two equal exposures ($r = 1$). Usually the rms fluctuations of the ratio (or difference) are calculated from a uniformly illuminated part of the image. We use non-uniform images and sort the pixels in groups with approximately equal signal before calculating σ_r^2. Thus the method works for both smooth intensity distributions and for structured images, e.g. quartz lamp spectra. The program is `ratio3.pro`.

Non-linearity has a strong effect on the gain calculation. Using (1), we can see that the product $\sigma_0^2 S$ depends on the signal as $1 + 5kS$ (to the first order). Thus, a 1% non-linearity causes 5% error in the gain measurement.

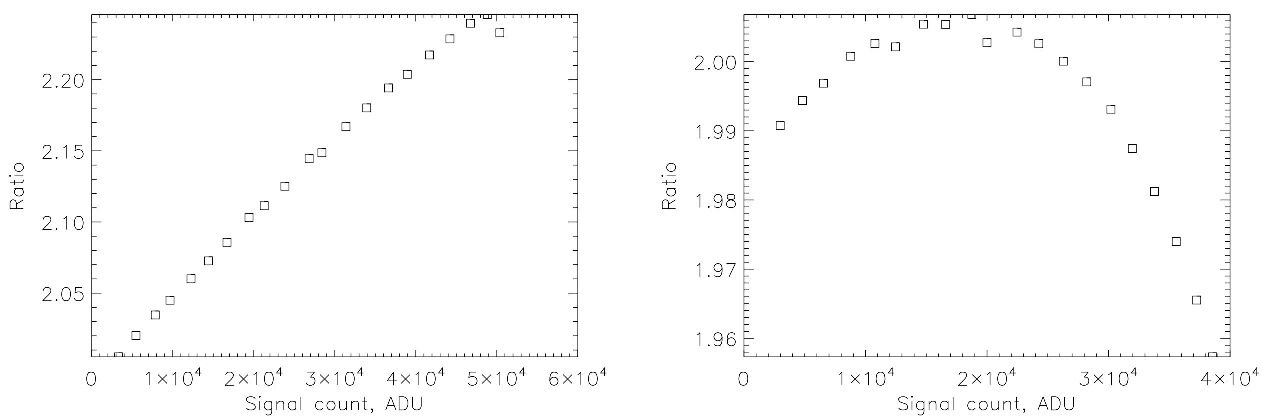

Figure 5: Ratio of two exposures ft0035/ft0036 in the right quadrant as a function of the signal level in the longest exposure. Left: before applying the non-linearity correction, right: corrected.

Figure 5 shows the effect of the non-linearity correction. The systematic dependence of the ratio on the signal level is reduced from $\sim 12\%$ to 1% for signal levels to to 20 kADU. At higher signals the correction is not accurate. Figure 6 illustrates the effect of non-linearity correction on the gain calculation. The most accurate and consistent gain measurements are obtained from the ratio of equal unsaturated exposures (Fig. 7).

Table 1 lists results of gain and RON measurements in different regimes using ratios of both equal and unequal exposures. We give the last two digits of the file names and the exposures in seconds. The RON is given in ADU rms, calculated from the overscan region in the "denominator" file (excluding the first and last overscan columns). For each image pair and each amplifier, the gain vs. signal

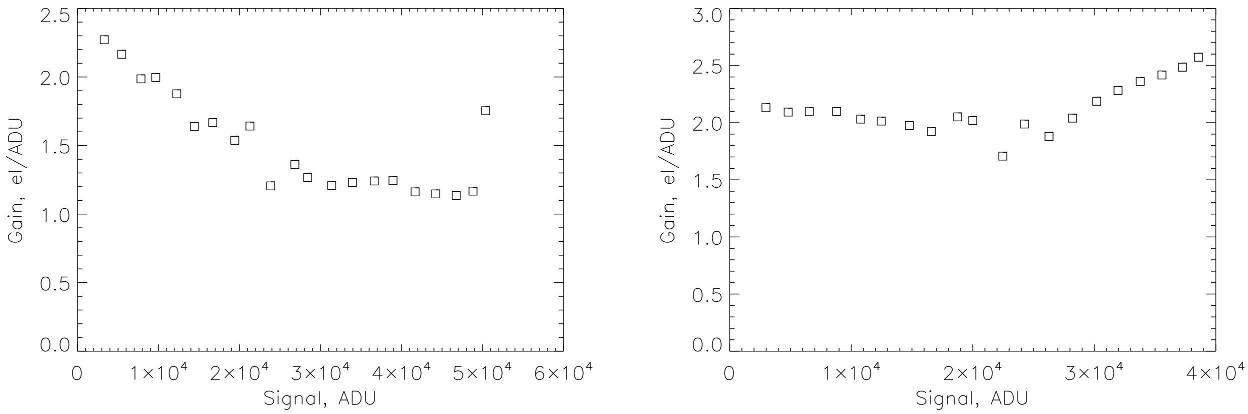

Figure 6: Dependence of the gain on signal level for the ratio of the same exposures as in Fig. 5. Left: without non-linearity correction, right: corrected.

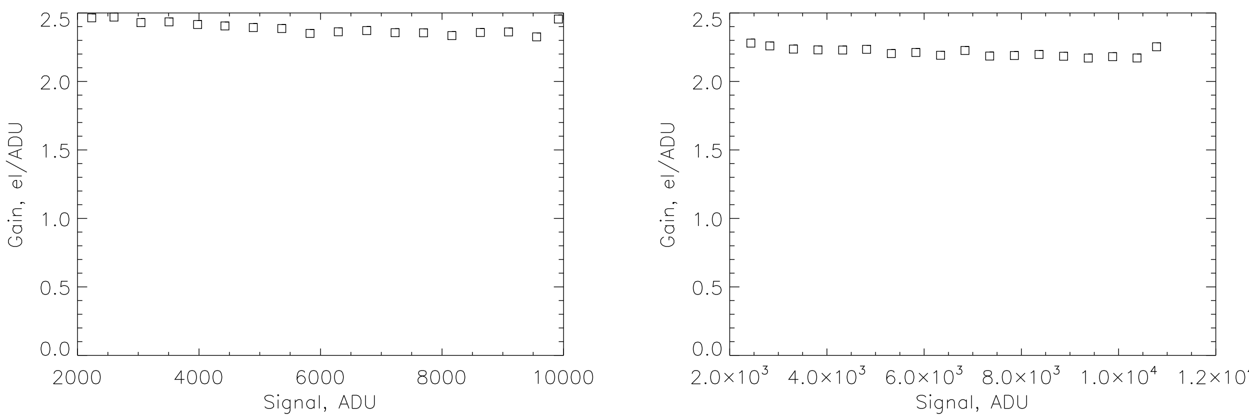

Figure 7: Dependence of the gain on the signal level, upper-left amplifier. Results from the ratios of equal exposures with smooth illumination (paper). Left: ft0010/ft0009, 2x2, fast mode. Right: ft0032/ft0025, 2x2, normal mode.

curve is obtained. Sometimes the first and last points show large deviations, possibly caused by excessive intensity range in the 1st bin and spikes or blemishes in the last one. The listed gain is averaged between 2-nd and 5th bins. The signal (in kADU) is averaged over the same bins in the 2nd (denominator) file.

The examination of the Table shows that after correction for the non-linearity, the gain measurements are very consistent. The gain does not depend on the image binning. Strangely, we measure increased noise in the fast mode without binning, compared to 2x2; no such effect is seen in the normal mode. The gains in the normal and fast modes are very similar.

The program `noise2.pro` is used to evaluate periodic components in the readout noise. For each

Table 1: RON and gain measurements

Image, Binning	Files	Exp., s	Upper-left			Upper-right		
			RON	Gain	S, kADU	RON	Gain	S, kADU
Paper Fast 2x2	17/18	4/2	2.97	2.511	0.65	2.98	2.106	0.96
	18/19	2/1	2.95	2.535	0.35	2.86	2.042	0.54
	10/9	10/10	2.94	2.436	3.30	2.90	2.103	4.85
	19/20	1/0.5	2.97	2.540	0.20	2.92	2.121	0.30
Image Fast 1x1	37/38	1/1	3.69	2.588	1.51	3.40	2.190	1.92
	38/39	1/0.5	3.56	2.583	0.76	3.32	2.191	0.96
	36/37	2/1	3.72	2.556	1.51	3.38	2.169	1.92
	35/36	4/2	3.71	2.477	3.02	3.52	2.080	3.86
Paper Normal 2x2	30/31	1/0.5	1.92	2.239	0.25	2.16	1.955	0.35
	26/25	20/10	1.98	2.201	3.59	2.23	1.878	5.60
	25/28	10/4	1.91	2.237	1.41	2.13	1.921	2.32
	28/29	4/2	1.94	2.279	0.71	2.18	1.941	1.17
	29/30	2/1	1.93	2.293	0.36	2.16	1.975	0.59
	32/25	10/10	1.98	2.222	3.59	2.23	1.916	5.90
Image Normal 1x1	58/56	1/1	1.87	2.391	1.67	2.04	2.056	2.10

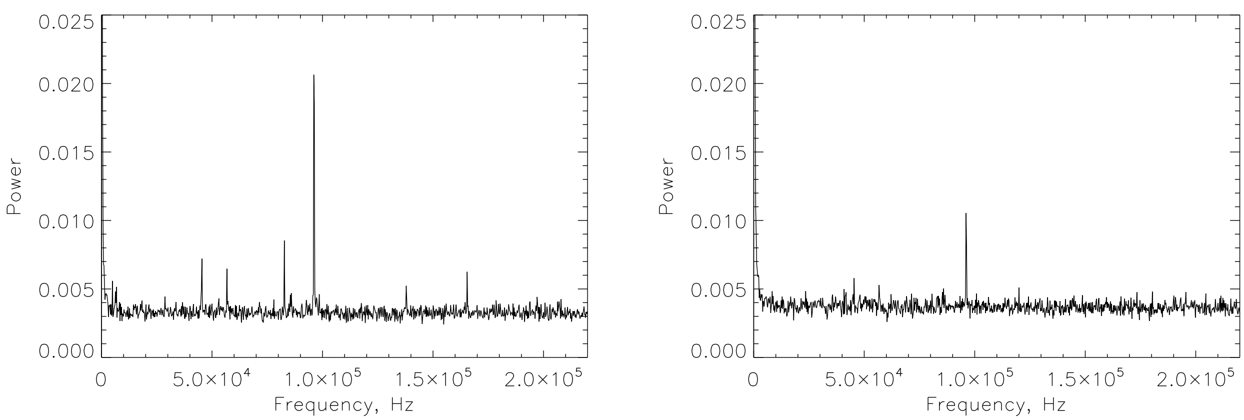

Figure 8: Power spectra of the noise in the bias image ft0043, averaged over all lines. The left and right amplifiers are plotted on left and right, respectively.

amplifier, the average line is subtracted from all lines, the result is Fourier-transformed, and the power spectrum is averaged for all lines. We processed the bias image ft0043 (fast mode, 1x1) using only upper 100 lines, to reduce the effect of weak parasitic light during readout. Pixel frequency of 440 kHz is assumed to convert spatial spectra into temporal frequencies (Fig. 8). Interestingly, the left amplifier has a stronger periodic noise, which however contributes negligibly to the total variance. On the other hand, the spectra rise sharply at low frequency; the rise apparently continues on time scales longer than the line readout time. This flicker-noise component causes horizontal "streaks" in the bias images (Fig. 1, right). The flicker component does contribute substantially to the overall signal variance. Indeed, the "noise floor" rms variance calculated from the median level of the power spectra (white noise only) is about 1.5 times smaller than the total variance along lines or columns. The results for ft0043 are

```
 ft0043  Lines rms     Columns rms Noise floor
Left     2.598         2.945      1.787
Right    2.766         3.321      1.898
```

Table 2: Readout modes summary

Mode	Readout time	Upper-left		Upper-right	
	s	RON, el	Gain el/ADU	RON el	Gain el/ADU
Normal 1x1	37	4.5	2.39	4.2	2.05
Normal 2x2	14	4.3	2.23	4.1	1.92
Fast 1x1	22	9.6	2.59	7.4	2.19
Fast 2x2	10	7.5	2.53	6.1	2.10

5 Binning and ROI

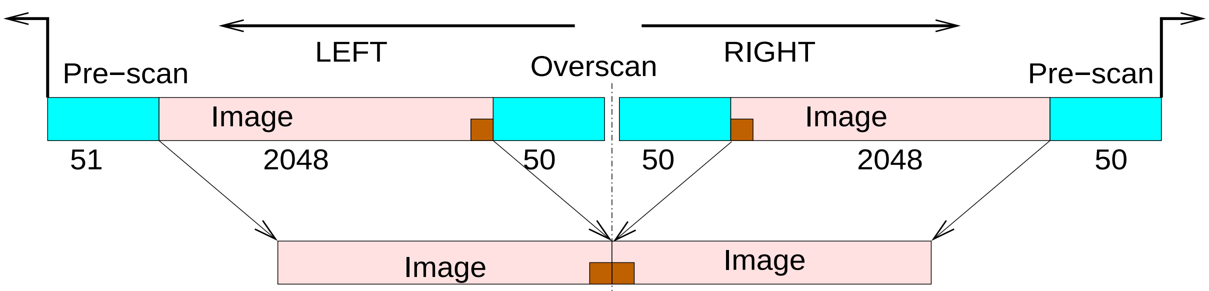

Figure 9: Clocking and binning. Schematic representation of one CCD line with pre- and over-scan pixels in blue, image pixels in pink. The two image sections join at the center. It is important to have bin limits (brown boxes) coincident with the limits of the image sections.

The two CCD halves are clocked together. The pre-scan sections have physical length of 51 and 50 pixels in the upper left and right serial registers, respectively (Fig. 9). This is a physical defect of all e2v 4K CCDs. For this reason, the left and right image sections are read with a 1-pixel time shift. This shift is taken into account in the TSEC and BSEC keywords in the no-binning case. However, it becomes apparent with binning. The start of the binning can be delayed by a certain number of clock cycles to make the last columns of each section (those that join at the center) coincide with the bin limits. For the 3x H-binning there is no need of such extra clock cycles because 51/3=17. On the other

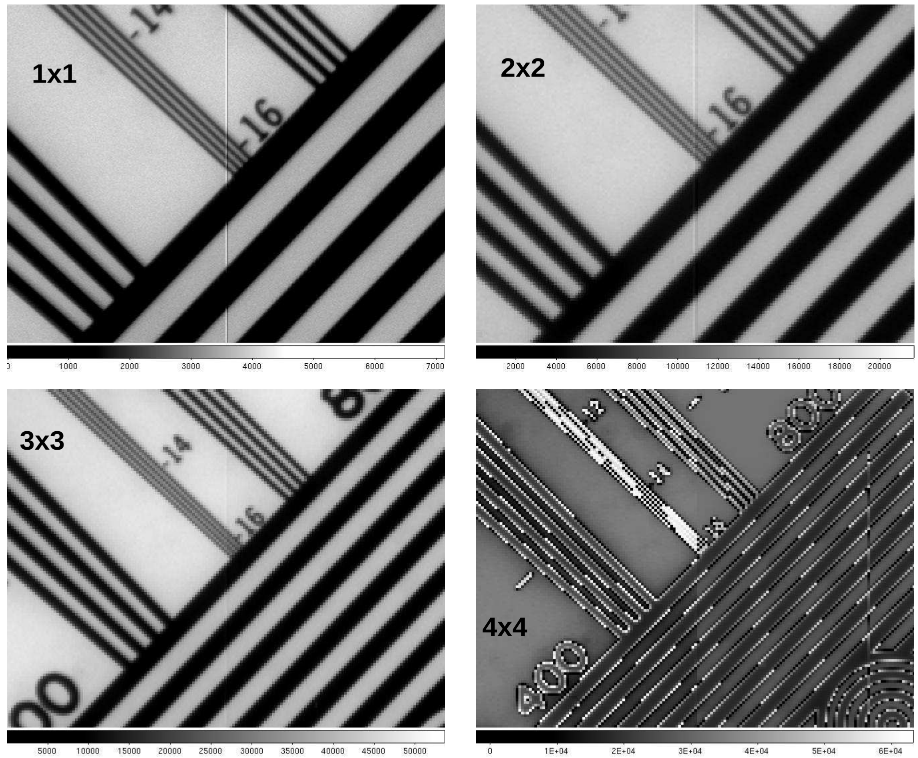

Figure 10: Fragments of test images near the center with different binning: 1x1, 2x2, 3x3, 4x4. Fast readout mode, full-frame. The 4x4 image is saturated. There is no spatial discontinuity between two CCD halves.

hand, with 4x H-binning we get a half-pixel mismatch between the bins and actual image sections because $50/4 = 12.5$. The matter is complicated further by a 1-pixel shift between fast and normal modes (the controller works in different modes) and when the region-of-interest, ROI, is selected.

Several test images with various binnings have been acquired. The images were "stitched" by the program `quad2.pro`: subtract median value of the overscan in each amplifier and put together the two halves of the image as indicated by the TSEC header keyword. For ease of perception, the right half is divided by 1.15 to equalize the gains. The resulting images had no discontinuity without binning and with 3x3 bining, but had two "dark" columns in the middle for 2x2 and 4x4 binning. Moreover, the relative shift between the two halves of the image depended on the ROI.

This problem has been fixed by M. Bonati. He repeated the binning tests on March 8, 2011 in four cases: fast and normal modes with and without ROI. The ROI parameters are [1000, 1, 1500, 4112], that is 1500 full columns starting from the column 1000, in un-binned CCD pixels. For each case, binnings of 1x1, 2x2, 3x3 and 4x4 were tested. In all 4 cases the stitched images show no discontinuity in the central column (Fig. 10). The files are located in `/data/20110308/`. Table 3 lists the file names and size of trimmed images. The `normroi0010` apparently had a 4x4 binnning. The image size in normal and fast modes matches, except the case of ROI with 3x3 binning.

It has been noted that the last (central) columns of the image have slightly different response in the two halves. That could be caused by a physical difference in the pixel size of the CCD (mask

Table 3: Binning and ROI tests on March 8, 2011

Case	Fast		Normal	
	File	Size	File	Size
Full 1x1	fast0005	4096x4112	normal0001	4096x4112
Full 2x2	fast0006	2048x2056	normal0002	2048x2056
Full 3x3	fast0007	1366x1370	normal0003	1366x1370
Full 4x4	fast0008	1024x1028	normal0004	1024x1028
ROI 1x1	fastroi0013	1500x4112	normroi0009	1500x4112
ROI 2x2	fastroi0014	749x2056	normroi0010	374x1028
ROI 3x3	fastroi0015	502x1370	normroi0011	500x1370
ROI 4x4	fastroi0016	374x1028	normroi0012	374x1028

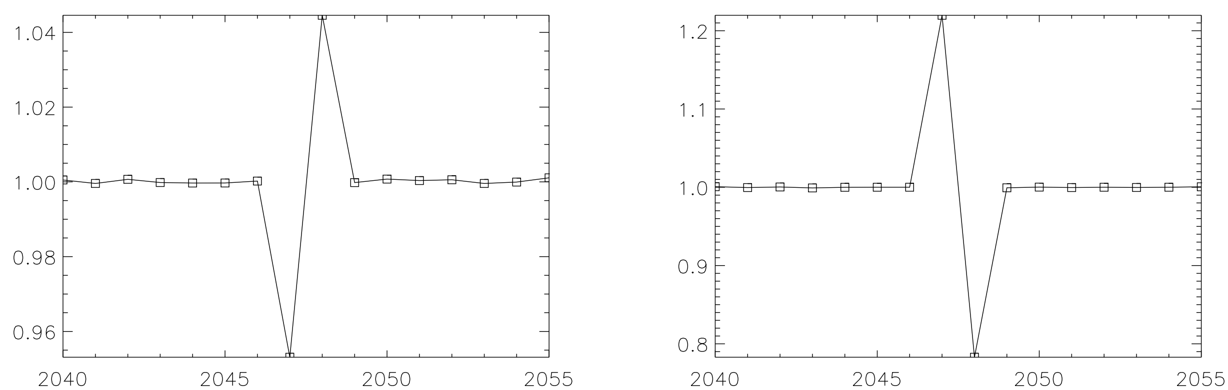

Figure 11: Horizontal cut of the stitched images ft0058 (left, 1x1 binning, normal mode) and ft0037 (right, 1x1 binning, fast mode) near the center (image section [*, 906:1240] averaged in Y). The right quadrant has been divided by 1.150/1.162 to equalize the gains.

shift during fabrication). However, the effect depends on the readout mode. In the fast mode, the last column of the left section is brighter, while in the normal mode it is dimmer. Figure 11 illustrates that the difference in the central-column response is about 4.5% and 22% in the normal and fast modes, respectively.

The region-of-interest (ROI) functionality has been tested. The actual image (as written to the disk) is symmetric about the center, even when the ROI isn't. This is caused by the need to clock both amplifiers synchronously. However, the TSEC keywords describe the actual ROI correctly, so the trimmed images can be asymmetric about the central column.

6 Charge transfer efficiency and cosmetics

The charge transfer efficiency (CTE) in the horizontal direction is readily evaluated by the fraction of the signal remaining in the first overscan column. These fractions for the left/right amplifiers are 0.4/0.6% in the image ft0037 (max. signal level 12 kADU) and 1.4/3.0% for the image ft0041 (max. signal 1.5 kADU above bias). This indicates that the CTE is lower at low signal levels, as typical for most CCDs. In the normal mode (ft0058, 1s exposure) the residual signal is 1.2/1.3%. The last column undergoes 2100 transfers, so a 3% residual signal means relative signal loss 1.4E-5 per transfer, or a CTE of 0.999986 per pixel. As the residual can be under 1%, the horizontal CTE is actually "five nines".

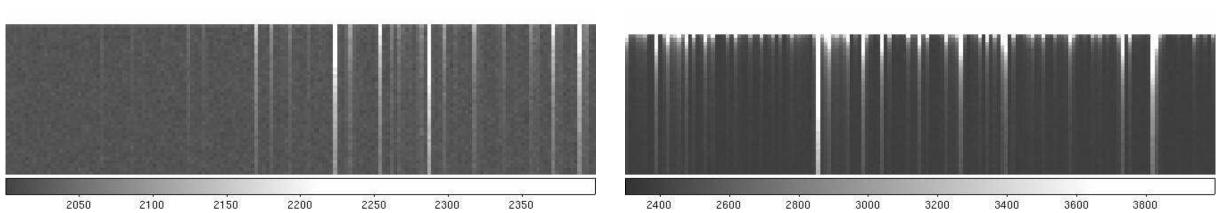

Figure 12: Fragments of the vertical overscan sections of the image ft0038 (1s exposure, fast mode, 1x1 binning). The signal level of the lowest image lines is about 7 kADU.

The CTE in the vertical direction could be evaluated in a similar way from the vertical overscan region. However, the overscan signal shows vertical "streaks" over several pixels, with an intensity changing from one column to another in a seemingly chaotic pattern (Fig. 12). In the darkest columns, there is no trace of residual charge in the 1st overscan pixel, indicating a perfect vertical CTE (so perfect that it can't be measured). Images of cosmic rays in the bias frames have sharp lower boundaries without any trace of "tails", indicating good vertical CTE at low signal levels. This is shown in Fig. 13, where we have combined 13 cosmic-ray events with visually sharp lower borders found in the lower lines of the 300-s dark exposure taken in normal mode (script `cosmic.pro`). The average signal is 800 ADU above background. The first dark pixel shows no excess signal at a level $< 0.5\%$, after 3804 vertical transfers on average. The vertical CTE equals one to within 1.3E-6.

The origin of the "tails" in the vertical overscan region remains unknown. They are not directly related to the illumination in each column. White streaks are seen even in the bias images, but only in the left amplifier, where the columns 606-631 stand out in the y-overscan.

The cosmetic quality of this particular CCD is quite good, but not perfect. In the left amplifier, there is a charge trap at X=566,567 and Y=3414 (pixels in the trimmed image), making for two bad columns. Interestingly, in the bias images we see a structure around those columns and bright streaks in the Y-overscan region below. In the right half, the most prominent defect is a charge trap at X=2305,2306 and Y=2460 which leaves a dark tail in those two columns below the trap. The tail extends for about 1000 pixels, then disappears. There are two localized detector blemishes at X,Y=(2347, 2526) and (2399, 2516).

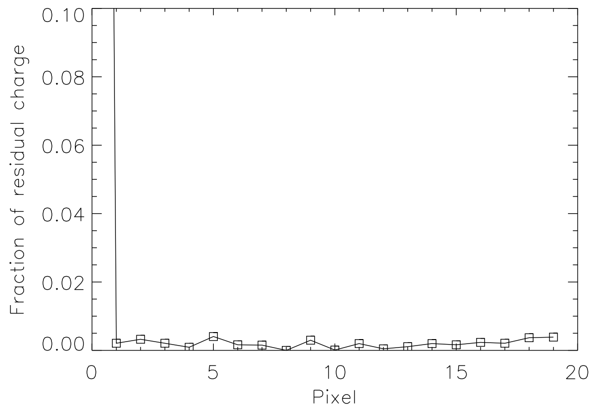

Figure 13: Combined trace of 13 cosmic-ray events showing no measurable charge in the 1st dark pixel. The cosmic-ray signal (pixel 0) is normalized to 1.

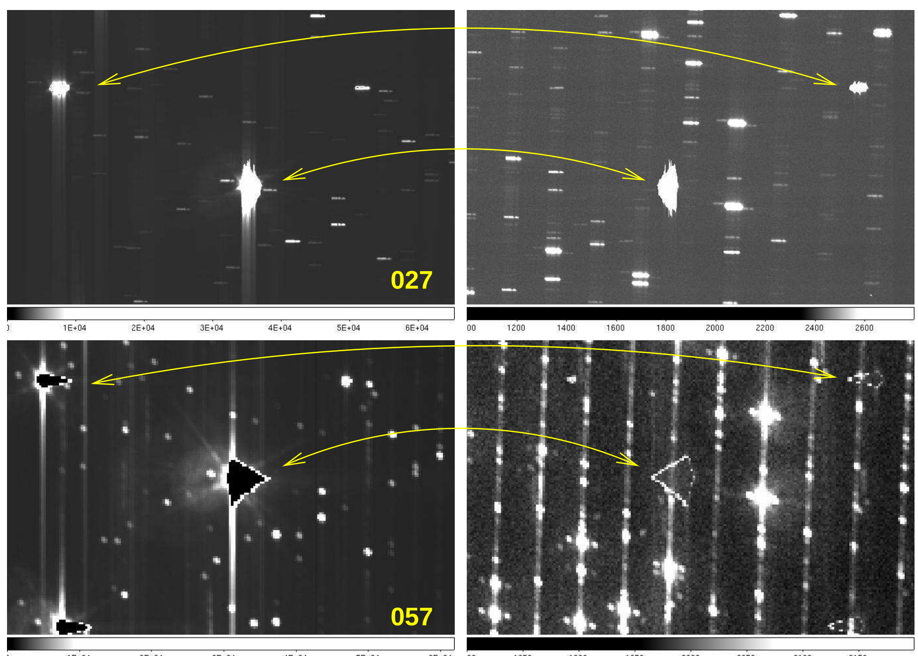

Figure 14: Matched segments of the Th-Ar comparison spectra showing saturated Ar lines on the left (red wavelengths) and their "reflections" in the right amplifier (blue wavelengths, marked by yellow arrows). The spatial scale of both fragments is identical, while the intensity scales are different. Upper pair: qa031.0027, 10-s unbinned exposure. Lower pair: qa031.057, 1s exposure with 4x4 binning.

7 Cross-talk

During first tests of CHIRON with the engineering CCD in December 2010 we noticed that bright saturated lines in one quadrant leave traces at symmetric locations in another quadrant. This cross-talk was attributed at the time to the faulty quadrant of the engineering CCD. However, it is also seen with the science CCD.

The ccross-talk is illustrated in Fig. 14 using the data of March 9 taken at the telescope. In the upper image, the bright lines show a charge bleeding along columns, with the signal saturated at about 50 000 ADU. Matching pixels in the right amplifier have signal some 300 ADU higher than the background. The "reflections" of saturated lines are easily identified, they are located between the true echelle orders. If the cross-talk were linear, it would correspond to 300/5E4 = 0.6%. However, we do not see "reflections" of weaker, un-saturated lines. This may indicate that the cross-talk is non-linear and somehow related to the saturation.

In the lower image taken in the 4x4 binning mode we see a "numerical" saturation at 2^{16} (we use only 16 bits out of 18) as black patches inside strong lines. Interestingly, this feature is repeated in the "reflections" which highlight the contour of the staurated zones. We cannot explain this behavior, unless the cross-talk is produced by the ADC converter itself.

8 Conclusions

The CHIRON CCD detector with Monsoon Orange controller can now be used for science. The readout noise is ∼4 electrons in the normal mode and 7-10 electrons in the fast mode; it is slightly reduced when we bin the CCD. In both normal and fast modes the gain is from 2 to 2.5 electrons per ADU. The binning and ROI are functional.

The response of the detector to light is non-linear, reaching 10% non-linearity at ∼25 kADU. This non-linearity can be corrected to ∼1% with a simple formula. A better correction could possibly be developed, given more accurate measurements (the data at hand are affected at 1% level by the light-source temperature dependence). The correction does not work well beyond 25 kADU. This defines a practical saturation limit of ∼6E4 electrons, 1/4 of the nominal CCD full-well capacity of 2.7E5 electrons. This will probably not affect the CHIRON science since the signal per pixel will be well below 25 kADU even for bright stars.

Table 4: Compliance to the statement of work

Parameter	Requirement	Compliance
CCD temperature, °C	−100, stabilized	Pass
Number of working outputs	4	Not pass (2)
Charge transfer efficiency per clock (min.)	0.999990	Pass (H,V)
Noise (electron rms) at 50 kHz pixel time, max	3.5	Pass (4e @ 200kHz)
Noise (electron rms) at 1 MHz pixel time, max	6	Not pass (9e @ 440kHz)
Min. readout time (1 MHz pixel time), s	6	Not pass (22s)
Charge storage per pixel, el. (min.)	270 000	Not pass (60 000)
Linearity, % (max.)	0.5	Not pass (1% after corr.)

Although the CCD is now in a working condition, its overall characteristics are inferior to the performance of similar 4K e2v CCD cameras and, mostly, do not comply to the statement of work (Table 4).